IEEE Access
Multidisciplinary | Rapid Review | Open Access Journal

IEEE POWER & ENERGY SOCIETY SECTION

Received July 11, 2020, accepted July 24, 2020, date of publication July 31, 2020, date of current version August 13, 2020.

Digital Object Identifier 10.1109/ACCESS.2020.3013396

Optimization of Integrated Energy System Considering Photovoltaic Uncertainty and Multi-Energy Network

JINGJING ZHAI[1,2], XIAOBEI WU[1], SHAOJIE ZHU[3], BO YANG[3,4], AND HAOMING LIU[3], (Senior Member, IEEE)

[1]School of Automation, Nanjing University of Science and Technology, Nanjing 210094, China
[2]School of Electric Power Engineering, Nanjing Institute of Technology, Nanjing 211167, China
[3]College of Energy and Electrical Engineering, Hohai University, Nanjing 211100, China
[4]China Electric Power Research Institute Company Ltd., Nanjing 210003, China

Corresponding author: Haoming Liu (liuhaom@hhu.edu.cn)

ABSTRACT The access of photovoltaics can reduce the carbon emissions of the integrated energy system and can also improve the economics of terminal energy supply, but the uncertainty of photovoltaic output also brings greater challenges to the optimal operation of the system. This paper focuses on coordinated optimization for the multiple energy systems in consideration of demand response. Latin hypercube sampling and the K-means algorithm are used to generate acceptable scenarios to deal with the photovoltaic uncertainty. Demand response based on Time-of-Use (TOU) electricity price is employed to realize the peak load shifting, and in consequence to improve the system operation. The optimization objective is to minimize the operational cost, subject to the constraints of electric grids, natural gas grids, and hot water pipeline grids. Due to the nonconvex constraints of these grids, the constraints are relaxed by means of the mixed integer linear programming approach, and the whole problem is established as a mixed integer linear programming model. Case studies show that demand response in each energy system and the coordinated optimization between the multiple energy systems can reduce the operational cost of the whole system. Even though the photovoltaic uncertainty results in a higher operational cost, the system has a more reliable operating point.

INDEX TERMS Integrated energy systems, multiple energy stations, multiple energy flow model, photovoltaic uncertainty, demand response.

I. INTRODUCTION

Compared to the conventional energy supply, multiple energy sources and their coordinated operation in the integrated energy systems can improve the efficiency and the economics of the whole system and the terminal consumption [1]. It is a trend to coordinate multiple energy stations in an integrated energy system in consideration of users' higher requirements on energy consumption, and therefore it is significant to investigate the coordinated operation of the energy systems.

Combined cold heat and power (CCHP) units, gas boilers, electric boilers, heat pumps, electric refrigeration devices, power to gas devices, electric energy storages, heat storage tanks, and ice storage tank [2]–[5] are common devices in the integrated energy systems. CCHP units can be coal-based draw condensing and back pressure units [6], [7] as well as gas turbines and gas internal combustion engines [8], [9]. Different units can be used in different scenarios [10]. For example, coal-based draw condensing and back pressure units are usually used in large thermal power plants [11], and the gas turbines are usually deployed in medium-sized power plants [12]. With the development of manufacturing techniques, the gas turbines with small capacities become popular [13]. There have been many research studies on the physical models of the integrated energy systems. In consideration of different dynamic responses of electric networks, natural gas networks, and heating/cooling networks, different dynamic models are established to integrate the control systems [14]. The steady-state models are used in [15], [16] to obtain the optimal scheduling with the objective of system economics. Due to network limits, the impacts of the networks of the integrated energy systems are investigated [17]–[19]. For example, the impacts of the natural gas grids on the electric network are analyzed in [20], in which the gas flow in each pipeline is modeled by means of the piecewise linear programming approach. In [21], the thermal model and the

The associate editor coordinating the review of this manuscript and approving it for publication was Elizete Maria Lourenco.

hydraulic model of the hot water pipelines are investigated to obtain the optimal operational costs with the electric grids.

In addition to accurate system modeling, accurate representations of uncertainty and demand response also have a critical impact on entire system optimization. In the integrated energy systems, there are many energy sources with high uncertainty, resulting in negative impacts on system operation. In consideration of high uncertainty, many research studies investigate the impacts of renewable uncertainty on system operation [22]–[26]. A chance-constrained programming model is proposed to deal with scheduling electrothermal energy systems with wind power, and the model is transformed into mixed integer linear programming, which can be easily solved [27]. With the upper level used to maximum the utility benefits and the lower level used to maximum the social benefits, a two-stage stochastic model is established to schedule the system in consideration of wind power [28]. In consideration of uncertain states of storages in the integrated energy system, [21] investigates a robust model for integrated power, gas and heat grids. A novel method based on information gap decision theory to evaluate a profitable operation strategy is proposed in [29] and [30], and furthermore demand response is considered in [30].

The integrated energy systems include multiple kinds of loads, e.g., gas loads and power loads. Compared to one conventional isolated system, loads in the integrated energy systems can be scheduled [31], [16]. Demand response of these loads can contribute to the peak load shifting, which makes the entire system more economic [32]. Interactions between different energy loads are analyzed in [33], and a game-based demand response in consideration of energy hubs are discussed. [34] focuses on the economic dispatch of the integrated energy systems with demand response.

At present, there are many research studies on modeling and scheduling of a single energy station. However, few studies focus on multiple energy stations and the impacts of their interdependency on the entire system operation. This paper focuses on coordinated scheduling for the integrated energy system with multiple energy hubs in consideration of photovoltaic uncertainty and demand response. Latin hypercube sampling and the K-means algorithm are used to generate scenarios representing photovoltaic outputs, and demand response is based on Time-of-Use (TOU) electricity prices. Multiple energy stations and their interactions are modeled as a group of mix integer linear constraints. The impacts of different photovoltaic outputs and demand responses on the integrated energy systems with the multiple energy stations are investigated.

II. INTEGRATED ENERGY SYSTEM WITH MULTIPLE ENERGY STATIONS

Fig. 1 is a multi-energy network topology of a comprehensive energy system demonstration project in Zhejiang Province. It shows a geographic map of an integrate energy system with five energy stations, and the power load, gas load, and cooling/heating load in each region with different colors are

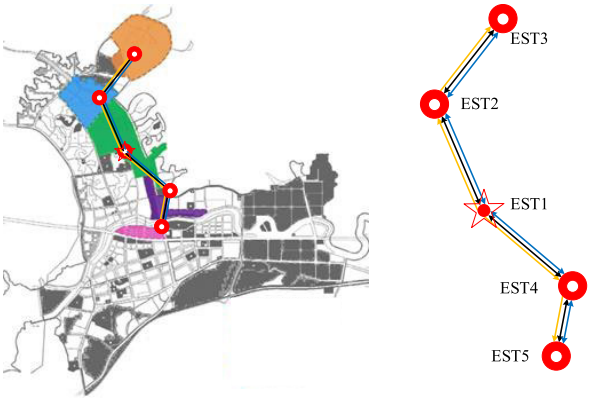

FIGURE 1. Geographical junction diagram of regional energy network.

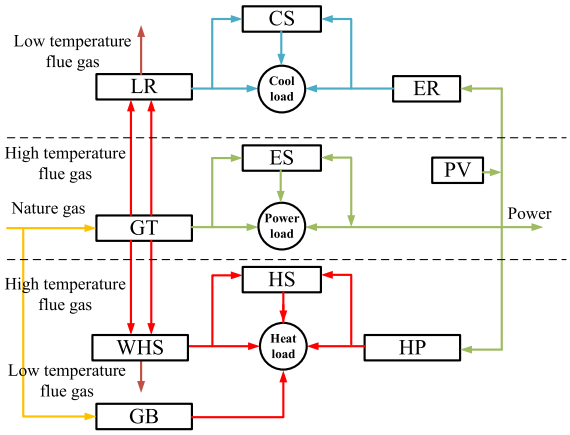

FIGURE 2. Flow chart of multi-energy supply system of an energy station.

supplied by each energy station. Fig. 2 shows the topology of five energy stations.

Single energy station equipment consists of: CCHP unit, gas boiler (GB), multiple energy storage equipment, electric refrigeration (ER), heat pump (HP), roof photovoltaic (PV) power generation device. Among them, CCHP units are composed of gas turbines (GT), lithium bromide refrigeration (LR), and waste heat recovery systems (WHS). Multiple energy storage equipment includes electric energy storage (ES), heat energy storage (HS), and cold energy storage (CS). The No.1 energy station is connected to the external power grid and the natural gas network.

III. OPTIMIZED OPERATION MODEL

A. OBJECTIVE FUNCTION

The optimization objective for the coordinated scheduling of the integrated energy system is listed in (1). The objective is to minimize the entire operational costs. Because PV uncertainty is included, the optimization objective is expressed as min-max formulation. C_F is the fuel cost, C_E is the cost of net electricity in the integrated energy system, C_S is the restart cost, C_M is the maintenance cost, and C_R is the revenues from demand response. The term 2.a is the fuel cost of CCHP, 2.b is the fuel cost of gas turbines, 3.a is the cost of purchasing electricity of the integrated energy system from the external

grid, 3.b is the cost of selling electricity to the external grid. 4.a is the restart cost of CCHP, and 4.b is the restart cost of gas turbines.

$$\min_{x\in X, o\in O}\max_{w\in W}\left(C_F+C_E+C_S+C_M-C_R\right) \tag{1}$$

$$C_F=\underbrace{\sum_{t=1}^{T}\sum_{o=1}^{N_S}\left(c_f\cdot F_{b,o}^{\mathrm{g}}(t)\cdot\Delta t\right)}_{2.a}+\underbrace{\sum_{t=1}^{T}\sum_{o=1}^{N_S}\left(c_f\cdot F_{d,o}^{\mathrm{g}}(t)\cdot\Delta t\right)}_{2.b} \tag{2}$$

$$C_E=\underbrace{\sum_{t=1}^{T}\left(\underline{c}_e(t)\cdot\underline{P}_e^{\mathrm{e}}(t)\right)\cdot\Delta t}_{3.a}-\underbrace{\sum_{t=1}^{T}\left(\overline{c}_e(t)\cdot\overline{P}_e^{\mathrm{e}}(t)\right)\cdot\Delta t}_{3.b} \tag{3}$$

$$C_S=\underbrace{\sum_{t=1}^{T}\left(\sum_{o=1}^{N_S}c_{b,o}\cdot\left|o_{b,o}(t)-o_{b,o}(t-1)\right|\right)}_{4.a}+\underbrace{\sum_{t=1}^{T}\left(\sum_{o=1}^{N_S}c_{d,o}\cdot\left|o_{d,o}(t)-o_{d,o}(t-1)\right|\right)}_{4.b} \tag{4}$$

$$C_M=\sum_{t=1}^{T}\sum_{a=1}^{N_A}\left(c_a\cdot P_a(t)\cdot\Delta t\right) \tag{5}$$

$$C_R=\sum_{t=1}^{T}\sum_{o=1}^{N_S}c_R\cdot\left(P_{R,o}^{\mathrm{e}}(t)-P_{L,o}^{\mathrm{e}}(t)\right) \tag{6}$$

where $F_{b,o}^{\mathrm{g}}$ is fuel input rate of the gas turbine units;$F_{d,o}^{\mathrm{g}}$ is fuel input rate of the gas boilers;c_f is the price of natural gas; $o_{b,o}$ is starting-up and stopping status of gas turbine units; $o_{d,o}$ is starting-up and stopping status of gas boilers;$\underline{P}_e^{\mathrm{e}}$ and $\overline{P}_e^{\mathrm{e}}$ are power purchased and sold by the grid; $\underline{c}_e$ and $\overline{c}_e$ are purchasing and selling price of electricity to the grid;$c_{b,o}$ and $c_{d,o}$ are starting and stopping costs of gas turbine and gas boilers;c_a is equipment maintenance costs; c_R is income from the participation of the electric load to demand response; $P_{L,o}^{\mathrm{e}}$ is power load of energy station o; $P_{R,o}^{\mathrm{e}}$ is electric load of the energy station o after conducting demand response; T is the total time period in one day; N_S is set of energy station in IES; N_A. is number of equipment in IES.

B. DEVICE MODELING

1) CCHP UNIT

A CCHP unit includes a gas turbine (GT), a waste heat boiler (WHB), LiBr absorption refrigeration (LR). Its model is expressed as follows. Equation (7) represents the mathematical relation between the CCHP output and the gas consumption, (8) shows the relation of electricity generation and heating production of each CCHP system, (9) shows the relation between cooling production and heating production in each LiBr refrigeration unit. (10) shows the output constraint of the CCHP unit, (11) shows the constraint of cooling production from the CCHP system, (12) shows the minimum start-up and shut-down time constraint of the CCHP. (13) and (14) are the ramp-up and ramp-down constraints of the CCHP unit.

$$F_b^{\mathrm{g}}(t)=o_b(t)\cdot P_b^{\mathrm{e}}(t)\big/(LHV\cdot\eta_{\mathrm{b}}) \tag{7}$$

$$P_b^{\mathrm{h}}(t)=\beta_b\cdot P_b^{\mathrm{e}}(t) \tag{8}$$

$$P_r^{\mathrm{c}}(t)=P_r^{\mathrm{h}}(t)\cdot\eta_r \tag{9}$$

$$\underline{P}_b^{\mathrm{e}}\cdot o_b(t)\le P_b^{\mathrm{e}}(t)\le\overline{P}_b^{\mathrm{e}}\cdot o_b(t) \tag{10}$$

$$0\le P_r^{\mathrm{h}}(t)\le\min\left\{0.8\cdot P_b^{\mathrm{h}}(t),\bar{P}_r^{\mathrm{h}}\right\} \tag{11}$$

$$\begin{cases}\left(T_b^{\mathrm{on}}(t)-\overline{T}_b^{u}\right)\left(o_b(t-1)-o_b(t)\right)\ge 0\\ \quad o_b(t-1)=1\\ \left(T_b^{\mathrm{off}}(t)-\underline{T}_b^{u}\right)\left(o_b(t)-o_b(t-1)\right)\ge 0\\ \quad o_b(t-1)=0\end{cases} \tag{12}$$

$$P_b^{e}(t)-P_b^{e}(t-1)\le\left(2-o_b(t-1)-o_b(t)\right)\underline{P}_b^{e}+\left(1+o_b(t-1)-o_b(t)\right)\overline{P}_b^{\mathrm{u}} \tag{13}$$

$$P_b^{e}(t-1)-P_b^{e}(t)\le\left(2-o_b(t-1)-o_b(t)\right)\underline{P}_b^{e}+\left(1-o_b(t-1)+o_b(t)\right)\underline{P}_b^{\mathrm{u}} \tag{14}$$

where P_b^{h} and P_b^{e} is thermal output and electrical output of CCHP unit;LHV is low heating value of natural gas; β_b is the thermal power ratio of CCHP unit; η_{b} is generation efficiency of the gas turbine unit; η_r is absorption refrigeration efficiency of LiBr; T_b^{on} and T_b^{off} are starting-up and stopping time of gas turbine units; $\overline{T}_b^{u}$ and $\underline{T}_b^{u}$ are minimum starting and stopping time of gas turbine unit; P_r^{h} and P_r^{c} are input heat power and output cold power of LiBr absorption refrigeration; $\bar{P}_r^{\mathrm{h}}$ is the maximum input thermal power of LiBr unit; $\underline{P}_b^{e}$ and $\overline{P}_b^{e}$ are minimum and maximum electric output power of CCHP unit; $\overline{P}_b^{\mathrm{u}}$ and $\underline{P}_b^{\mathrm{u}}$ are maximum uphill and downhill speed of CCHP unit.

2) GAS BOILER

The gas boiler heats the medium water through the heat energy generated by natural gas combustion, and then transmits the heat energy to the users through hot water pipelines. The mathematical model can be expressed as follows. Equation (15) shows the relationship between the thermal output power and the fuel input rate of the gas boiler. (16) shows the output constraint of the gas boiler. (17) show the minimum start-up and shut-down time constraint of the gas boiler, and (18) and (19) represent the ramp-up and ramp-down constraints of the gas boiler, respectively.

$$F_d^{g}(t)=P_d^{\mathrm{h}}(t)\Big/LHV\cdot\eta_d \tag{15}$$

$$\underline{P}_d^{\mathrm{h}}\cdot o_d(t)\le P_d^{\mathrm{h}}(t)\le\overline{P}_d^{\mathrm{h}}\cdot o_d(t) \tag{16}$$

$$\begin{cases}\left(T_d^{\mathrm{on}}(t)-\overline{T}_d^{u}\right)\left(o_d(t-1)-o_d(t)\right)\ge 0 & o_d(t-1)=1\\ \left(T_d^{\mathrm{off}}(t)-\underline{T}_d^{u}\right)\left(o_d(t)-o_d(t-1)\right)\ge 0 & o_d(t-1)=0\end{cases} \tag{17}$$

$$P_d^{\mathrm{h}}(t) - P_d^{\mathrm{h}}(t-1) \le (2 - o_d(t-1) - o_d(t))\,\underline{P}_d^{\mathrm{h}} + (1 + o_d(t-1) - o_d(t))\,\overline{P}_d^{\mathrm{u}} \quad (18)$$

$$P_d^{\mathrm{h}}(t-1) - P_d^{\mathrm{h}}(t) \le (2 - o_d(t-1) - o_d(t))\,\underline{P}_d^{\mathrm{h}} + (1 - o_d(t-1) + o_d(t))\,\underline{P}_d^{\mathrm{u}} \quad (19)$$

where, η_d is efficiency of the gas boiler; P_d^{h} is thermal output of GB; $\underline{P}_d^{\mathrm{h}}$/and $\overline{P}_d^{\mathrm{h}}$ are minimum and maximum thermal output of GB; T_d^{on} and T_d^{off} are starting-up and stopping time of gas boilers; $\overline{T}_d^{u}$ and $\underline{T}_d^{u}$ are minimum starting and stopping time of gas boiler; $\overline{P}_d^{\mathrm{u}}$ and $\underline{P}_d^{\mathrm{u}}$ are maximum up and down slope rate of GB.

3) ELECTRIC REFRIGERATION

The double-working-condition electric refrigeration devices have two working conditions: air conditioning refrigeration and ice making. When working in the ice making condition, it needs to work with the ice storage tank. Its mathematical model is expressed as follows. Formula (20) shows the function of the cooling production with regard to power into the electric refrigeration, and (21) shows the limits of cooling production.

$$P_v^{\mathrm{c}}(t) = P_v^{\mathrm{e}}(t) \cdot \eta_{\mathrm{v}} \cdot COP_{\mathrm{v}} \quad (20)$$

$$\underline{P}_v^{\mathrm{c}} \le P_v^{\mathrm{c}}(t) \le \overline{P}_v^{\mathrm{c}} \quad (21)$$

where, P_v^{e} and P_v^{c} are input electric power / output cold power of the electric refrigeration units; η_{v} is efficiency of the electric cooling; COP_{v} is coefficient of electric refrigeration; $\underline{P}_v^{\mathrm{c}}$ and $\overline{P}_v^{\mathrm{c}}$ are minimum and maximum cooling output of electric refrigeration;

4) HEAT PUMP

The heat pumps are divided into geothermal pumps and air source heat pumps. The heat pump can collect the heat energy of the earth through high-quality electric energy to get low-quality heat energy, which is much higher than the efficiency of the electric heating boiler. It is a kind of high efficiency electric-heat conversion device, where (22) shows the function of the cooling production with regard to power into the electric refrigeration, and (23) shows the limits of heat production.

$$P_w^{\mathrm{h}}(t) = P_w^{\mathrm{e}}(t) \cdot \eta_w \cdot COP_w \quad (22)$$

$$\underline{P}_w^{\mathrm{h}} \le P_w^{\mathrm{h}}(t) \le \overline{P}_w^{\mathrm{h}} \quad (23)$$

where, P_w^{e} and P_w^{h} are input electric power and output thermal power of the heat pump; η_w are efficiency of the heat pump; COP_w is heating coefficient of heat pump; $\underline{P}_w^{\mathrm{h}}$ and $\overline{P}_w^{\mathrm{h}}$ are minimum and maximum heat output of the heat pump.

5) ENERGY STORAGE

Each energy station includes different kinds of storages, e.g., battery, heat storage tank and ice storage tank. The model can be expressed as follows. Formula (24) is the charging and discharging model of the storage, (25) represents the state of charge constraint of the electric heating and cooling multi-energy storage, (26) represents the power constraint

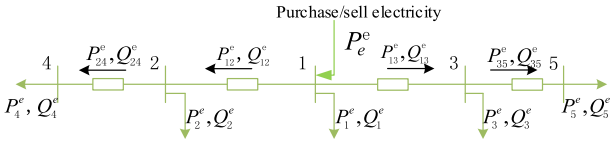

FIGURE 3. Topology of electric network between different energy stations.

of charge and discharge of the multiple energy storage, and (27) represents the constraint of energy storage state at the beginning and the end.

$$E_{(\cdot)}(t) = E_{(\cdot)}(t-1) \cdot (1 - \delta_{(\cdot)} \cdot \Delta t) + \left(P_{(\cdot)}^{\mathrm{cha}}(t) \cdot \eta_{(\cdot)}^{\mathrm{cha}} - \frac{P_{(\cdot)}^{\mathrm{dis}}(t)}{\eta_{(\cdot)}^{\mathrm{dis}}} \right) \cdot \Delta t \quad (24)$$

$$SOC_{(\cdot)}^{\min} \le \frac{E_{(\cdot)}(t)}{E_{(\cdot)}^{\mathrm{r}}} \le SOC_{(\cdot)}^{\max} \quad (25)$$

$$\begin{cases} 0 \le P_{(\cdot)}^{\mathrm{cha}}(t) \le \gamma_{(\cdot)}^{\mathrm{cha}} \cdot E_{(\cdot)}^{\mathrm{r}} \\ 0 \le P_{(\cdot)}^{\mathrm{dis}}(t) \le \gamma_{(\cdot)}^{\mathrm{dis}} \cdot E_{(\cdot)}^{\mathrm{r}} \end{cases} \quad (26)$$

$$E_{(\cdot)}(0) = E_{(\cdot)}(T) \quad (27)$$

where, $P_{(\cdot)}^{\mathrm{cha}}$ and $P_{(\cdot)}^{\mathrm{dis}}$ are charge and discharge power of energy storage; $\eta_{(\cdot)}^{\mathrm{cha}}$ and $\eta_{(\cdot)}^{\mathrm{dis}}$ are charge and discharge efficiency of the energy storage; $SOC_{(\cdot)}^{\min}$ and $SOC_{(\cdot)}^{\max}$ are minimum and maximum state of charge of energy storage; $E_{(\cdot)}$ is energy storage of electrical, thermal and cold energy storage; $E_{(\cdot)}^{\mathrm{r}}$ is rated energy storage of energy storage;$\gamma_{(\cdot)}^{\mathrm{cha}}$ and $\gamma_{(\cdot)}^{\mathrm{dis}}$ are maximum charge and discharge ratio of energy storage;$\delta_{(\cdot)}$ are self-consumption rate of energy storage; $E_{(\cdot)}(0)$ and $E_{(\cdot)}(T)$ are energy storage at the beginning and end of the day.

6) PURCHASE/SELL ELECTRICITY

Only one energy station is connected to the large power grid, and this energy station is No. 1 energy station. The transmission power of the tie line in integrated energy system is limited by the capacity of transformer.

$$\begin{cases} \underline{P}_x^{\mathrm{e}} \le \overline{P}_e^{\mathrm{e}}(t) \le \overline{P}_x^{\mathrm{e}} \\ \underline{P}_x^{\mathrm{e}} \le \underline{P}_e^{\mathrm{e}}(t) \le \overline{P}_x^{\mathrm{e}} \end{cases} \quad (28)$$

where, $\underline{P}_x^{\mathrm{e}}$ and $\overline{P}_x^{\mathrm{e}}$ are minimum and maximum power purchased and sold by the grid.

C. NETWORK MODELING

1) ELECTRICITY NETWORK

The topology of the electric grid between different energy stations is a radial distribution network, it is shown in Fig. 3.

It is assumed that No. 1 energy station is the reference node of the integrated energy system. The reference energy station is directly connected to the external grid, and can have direct power interactions with the external grid. Since the distance between multiple energy stations is less than 5 km, the loss of distribution network is ignored in this paper. The power flow model of the distribution network is expressed as follows:

$$P_i^e = -\sum\nolimits_{j \in \Omega(i)} P_{ij}^{\mathrm{e}}(t) + P_e^e \quad (29)$$

where, P_i^e is input electric power of energy station i; P_{ij}^{e} is active power of the power line between node (energy station) i and j; P_e^e is the synthesis of purchasing and selling power in power grid.

The model of the electric network can be expressed as follows [35]:

$$U_i^2(t) - U_j^2(t) = 2\left(r_{ij}P_{ij}^{\mathrm{e}}(t) + x_{ij}Q_{ij}^{\mathrm{e}}(t)\right) \tag{30}$$

where U_i is voltage of node (energy station) i; r_{ij} is resistance of power line ij; x_{ij} is reactance of power line ij; Q_{ij}^{e} is reactive power of the power line between node (energy station) i and j; Substitute U_i^2 with V_i to obtain the following equation [36]:

$$V_i(t) - V_j(t) = 2\left(r_{ij}P_{ij}^{\mathrm{e}}(t) + x_{ij}Q_{ij}^{\mathrm{e}}(t)\right) \tag{31}$$

where (31) is a linear model. In addition, the constraints with regard to voltage and line power should be satisfied as follows [37]:

$$\underline{V}_i \le V_i(t) \le \overline{V}_i \tag{32}$$

$$-\sqrt{2}S_l^{\mathrm{e}} \le P_{ij}^{\mathrm{e}}(t) + Q_{ij}^{\mathrm{e}}(t) \le \sqrt{2}S_l^{\mathrm{e}} l \in L, \quad t \in T \tag{33}$$

$$-\sqrt{2}S_l^{\mathrm{e}} \le P_{ij}^{\mathrm{e}}(t) - Q_{ij}^{\mathrm{e}}(t) \le \sqrt{2}S_l^{\mathrm{e}} l \in L, \quad t \in T \tag{34}$$

where (32) is the voltage constraint, and (33), (34) are the power flow limits for the line l. $\underline{V}_i$ and $\overline{V}_i$ are square of the minimum and maximum voltage allowed at node i; S_l^{e} is maximum allowable power of power line ij.

2) GAS NETWORK

In the natural gas distribution network, the temperature change and the dynamic process of the natural gas transmission are often ignored. If the elevation of the network is assumed to be at the same level, equation (35) shows the pressure drop equation of natural gas network [20].

$$F_{ij}(t) \cdot \left|F_{ij}(t)\right| = C_{ij}^2\left(\tau_i^2(t) - \tau_j^2(t)\right) \quad \forall i, j, t \tag{35}$$

where (35) is a nonlinear and nonconvex equation, and it can be transformed into a mixed integer linear model as follows (36)-(39). F_{ij} is natural gas flow rate of natural gas pipeline ij; C_{ij} is pipeline parameters of natural gas pipeline ij;τ_i is pressure of node (energy station) i; Substitute τ_j^2 with π_i to obtain the following equation.

$$\sum_k \left(A_g^k(t) \cdot f_g^k(t) + B_g^k(t) \cdot \nu_g^k(t)\right) = C_{ij}^2\left(\pi_i(t) - \pi_j(t)\right) \quad \forall t, g, (i,j) \in g \tag{36}$$

$$\sum_k \nu_g^k(t) = 1 \quad \forall t, g \tag{37}$$

$$\nu_g^k(t)\underline{f}_g^k \le f_g^k(t) \le \nu_g^k(t)\overline{f}_g^k \quad \forall t, g, k \tag{38}$$

$$F_{ij}(t) = \sum_k f_g^k(t) \quad \forall t, g, (i,j) \in g \tag{39}$$

where A_g^k and B_g^k are section linearization parameters of natural gas pipeline; f_g^k is linearization section flow of the natural gas pipeline section; ν_g^k is binary variable of segment linearization for gas flow in pipeline.

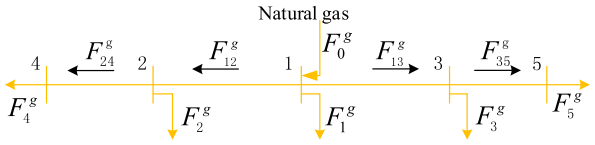

FIGURE 4. The diagram of the natural gas pipeline.

The natural gas pressure of each node is mainly related to the natural gas consumption, and the pressure of each node needs to meet the pressure constraint (40).

$$\underline{\pi}_i \le \pi_i(t) \le \overline{\pi}_i \tag{40}$$

where $\underline{\pi}_i$ and $\overline{\pi}_i$ are square of the minimum and maximum value of the pressure at node i of the natural gas pipeline.

In the operation of natural gas pipeline between multi-energy stations, not only the pressure constraints of pipeline, but also the flow balance constraints of nodes should be meet, shown as equation (41).

$$F_i^g(t) = -\sum\nolimits_{j\in\Omega(i)} F_{ij}^g(t) + F_{01}^g(t) \tag{41}$$

where F_i^g is the amount of natural gas consumed by node i. F_{01}^g is natural gas purchased from outside by the integrated energy system.

The topology of the natural gas pipeline between different energy stations is shown in Fig. 4, only energy station 1 is directly connected to the urban natural gas pipeline.

3) HEAT NETWORK

The models of heat network include thermodynamic equations and hydraulic equations. The thermodynamic equations are listed as follows. Formula (42) and (43) are the thermal equations of hot water pipelines, (44) is the pipe temperature constraint. When the heat transfer mode of the hot water pipeline is constant flow and variable temperature, the heat equation of the hot water pipeline is linear.

$$\begin{cases} P_o^h(t) = C \cdot M_o(t) \cdot \left(T_o^{\mathrm{S}}(t) - T_o^R(t)\right) \\ T_j(t) = T_i(t)\,\phi_{ij}(t) \\ \left(\sum M_o^M(t)\right) T_o^M(t) = \left(\sum M_o^B(t)\,T_o^B(t)\right) \end{cases} \tag{42}$$

$$\begin{cases} T_i(t) = T_i'(t) - T_a \\ T_j(t) = T_j'(t) - T_a \\ \phi(t) = e^{-\lambda L_{ij}/CM_{ij}(t)} \end{cases} \tag{43}$$

$$\begin{cases} \underline{T_o} \le T_o(t) \le \overline{T_o} \\ \underline{M_{ij}} \le M_{ij}(t) \le \overline{M_{ij}} \end{cases} \tag{44}$$

where M_o is hot water flow of node o; T_o^{S} and T_o^R are supply and return water temperature of node o; C is the specific heat capacity of water;T_i and T_j are the temperature of nodes i and j after the equivalent; T_i' and T_j' are the actual measured temperatures of nodes i and j; ϕ_{ij} is the temperature drop coefficient of pipe ij; M_o^M and T_o^M are the hot water flow and

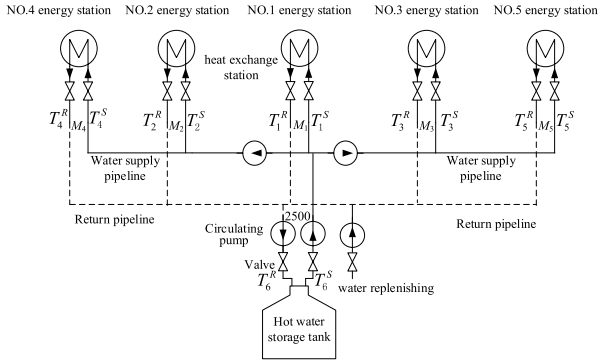

FIGURE 5. Thermal network topology.

temperature of the main pipeline; M_o^B and T_o^B are the hot water flow and temperature of the branch pipeline; λ is the pipeline parameter; L_{ij} is the pipe length;$\underline{T_o}$ and $\overline{T_o}$ are minimum and maximum allowable temperature of node o; $\underline{M}_{ij}$ and $\overline{M}_{ij}$ are minimum and maximum flow of pipeline ij.

The hydraulic equations are expressed as follows. where (45) shows the flow balance equation of each node and loop pressure drop equation in water pipeline. and the connections between nodes and loops are shown in Fig. 5.

$$\begin{cases} A_h(t) \cdot M_{ij}(t) = M_o(t) \\ B_h(t) \cdot M_{ij}^T(t)\, diag(K_{ij}) \left|M_{ij}(t)\right| = 0, \end{cases} \quad j = 1, \cdots, n_{st} \tag{45}$$

where A_h is the node incidence matrix; B_h is the loop incidence matrix; K_{ij} is the pressure drop coefficient of pipeline ij.

D. INTERNAL ENERGY BALANCE CONSTRAINT OF ENERGY STATION

Multiple energy stations are included in the regional integrated energy system. Each energy station is connected by the energy pipe network, and the energy can be transmitted among multiple energy stations to realize the efficient use of energy. (46) is the power balance constraint in each energy station, (47) is the heat balance constraint in each energy station, equation (48) is the cold balance constraint in each energy station, and equation (49) is the gas balance constraint in each energy station.

$$\begin{aligned} P_o^e(t) = {} & P_{L,o}^{\mathrm{e}}(t) - \left[P_{b,o}^{\mathrm{e}}(t) + P_{pv,o}(t) - P_{wp,o}^{e}(t)\right. \\ & \left. - P_{h,o}^{\mathrm{e}}(t) - P_{v,o}^{\mathrm{e}}(t) - P_{es,o}^{\mathrm{cha}}(t) + P_{es,o}^{\mathrm{dis}}(t)\right] \end{aligned} \tag{46}$$

$$\begin{aligned} P_o^h(t) = {} & P_{L,o}^{\mathrm{h}}(t) - \left[P_{b,o}^{\mathrm{h}}(t) + P_{d,o}^{\mathrm{h}}(t) - P_{r,o}^{\mathrm{h}}(t)\right. \\ & \left. + P_{h,o}^{\mathrm{h}}(t) - P_{hs,o}^{\mathrm{cha}}(t) + P_{hs,o}^{\mathrm{dis}}(t)\right] \end{aligned} \tag{47}$$

$$P_o^c(t) = P_{L,o}^{\mathrm{c}}(t) - \left[P_{r,o}^{\mathrm{c}}(t) + P_{v,o}^{\mathrm{c}}(t) - P_{cs,o}^{\mathrm{cha}}(t) + P_{cs,o}^{\mathrm{dis}}(t)\right] \tag{48}$$

$$F_o^g(t) = F_{L,o}^{\mathrm{g}}(t) + F_{b,o}^{\mathrm{c}}(t) + F_{d,o}^{\mathrm{h}}(t) \tag{49}$$

where P_o^e is input electric power of energy station o; P_o^h is input thermal power of energy station o; P_o^c is input cold power of energy station o;F_o^g is natural gas input of energy station o.

IV. OPTIMIZATION MODEL

A. PV UNCERTAINTY

The integrated energy system faces many uncertainties on both the supply [38] and demand [39] sides. The paper starts from the supply side and considers the uncertainty of photovoltaic output. In our paper, we assume that the probability density distribution of photovoltaic power generation satisfies Gaussian distribution [40], [41] for the sake of exposition. However, it is worth pointing out that other probability density distributions can be used in this paper. The Gaussian distribution is shown as follows.

$$f\left(\tilde{P}_{pv}\right) = \frac{1}{\sqrt{2\pi}\sigma_{pv}} \cdot \exp\left[-\frac{\left(P_{pv} - \tilde{P}_{pv}\right)^2}{2\sigma_{pv}^2}\right] \tag{50}$$

where $\tilde{P}_{pv}$ is the expected value of forecasting PV power, σ_{pv} is the standard deviation of forecasting errors, and P_{pv} is the forecasting PV power (kW).

Robust optimization is used to deal with PV uncertainty, and it is used to obtain the optimal solution against the worst scenario. This paper uses the following steps to generate the PV output scenarios: 1) With the forecasted PV outputs (Fig. 6 a) and the probability density function of the forecasted errors, PV output scenarios (Fig. 6 b) are generated by means of Latin hypercube sampling method. 2) The K-means method is used to reduce the generated PV output scenarios, and N scenarios (Fig. 6 c) are selected. 3) Sort the scenarios ascendingly, and select the N*(0.5-0.5*n%)th and N*(0.5+0.5*n%)th values as the lower and upper bounds of PV outputs, respectively. The range of the parameter n is (0, 100). A larger n denotes that the corresponding strategy is more robust.

Based on the above steps, the uncertainty range of PV power can be determined as follows:

$$P_{pv}(t) \in \left[P_{pv}(t), \bar{P}_{pv}(t)\right] \tag{51}$$

where $P_{pv}(t)$ and $\bar{P}_{pv}(t)$ are the lower and upper bounds, respectively.

B. OPTIMIZATION ALGORITHM

In consideration of PV uncertainty, robust optimization model is used to deal with the worst scenario when scheduling the system. The robust optimization model is presented as follows [42]–[44]:

$$\begin{cases} \min\limits_{x,o} \max\limits_{w} C(x, o, w) \\ \text{s.t.} G(x, o, w) \le 0 \\ x \in X \\ o \in O \\ w \in W \end{cases} \tag{52}$$

where x and o are control variables, x is the continuous variable, o is the binary variable, w is the stochastic variable,

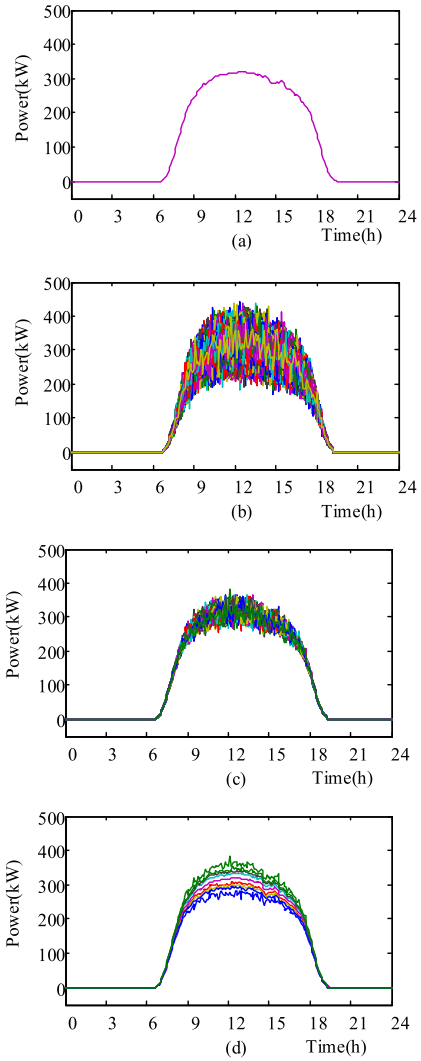

FIGURE 6. PV scenario generation.

$C(x, o, w)$ is the optimization objective, $G(x, o, w)$ is the constraint, X and O are feasible solution set of x and o, respectively. W is set of w, which is generated by using the method introduced in 3.1. The corresponding objective and the constraints are established in the previous section. The entire model is a mixed integer linear programming model, which is solved by Gurobi associated with YALMIP.

V. CASE ANALYSIS

A. BASIC DATA

A multi-energy network with five energy stations in Zhejiang Province of China is used to validate the proposed model, and its topology is shown in Fig. 1. The cooling, heating, power load, and the predicted photovoltaic output in the energy stations are shown in Fig. 7 a, b, c, and d, respectively. There are PVs in ES1, ES2, and ES3. In consideration of the limited geographical area of each energy station, it is assumed that the network topology in each energy station is not considered, and we only consider the network topologies between different energy stations. Due to different user types, the five energy stations have different peak and valley

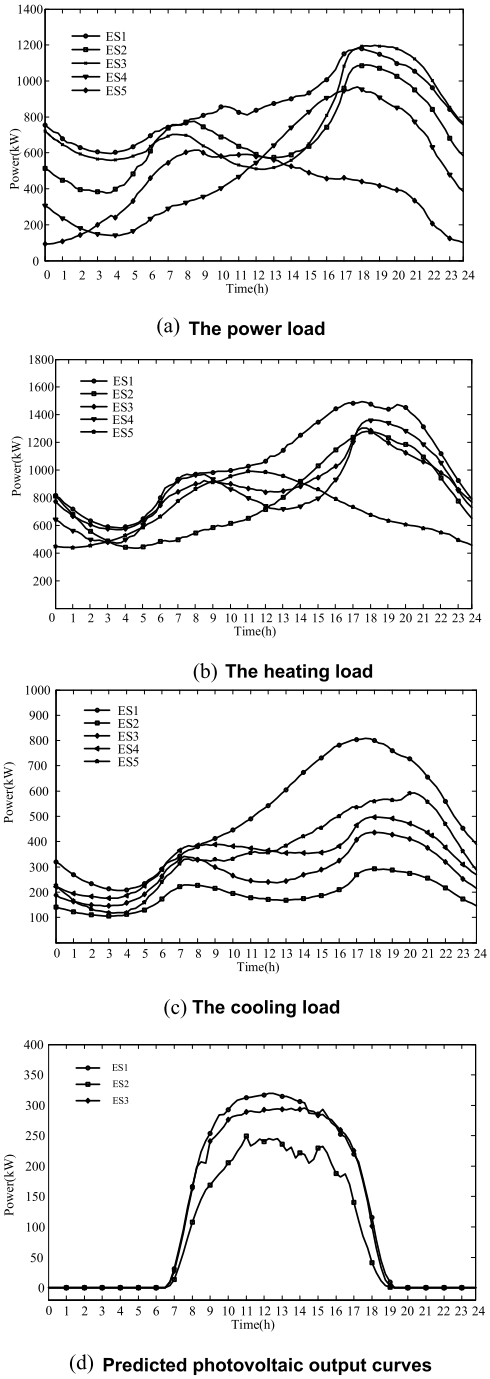

FIGURE 7. The loads curves of each energy station.

load times. There are 96 intervals in a day, and each interval is 15 minutes. The equipment configuration of each energy station is listed in Table 1. The equipment parameters of each energy station are listed in Table 2. The parameters of energy storage equipment are listed in Table 3 [9]. The energy network parameters of each energy station are listed in Table 4. Time-of-use electricity price is used. The periods of low price are 0:00∼7:00 and 23:00∼24:00, the periods of high price are 7:00∼10:00, 15:00∼18:00, 21:00∼23:00, and the periods of peak price are 10:00∼15:00 and 18:00∼21:00.

TABLE 1. The equipment configuration of each energy station.

Equipment	1	2	3	4	5
CCHP	√	√	√	√	√
GB	√	√	√	√	×
ER	√	√	√	√	√
HP	√	√	√	×	√
PV	√	√	√	×	×
ES	√	√	×	×	×
HS	√	√	×	×	×
CS	√	×	×	√	√

TABLE 2. The equipment parameters of each energy station.

Equipment		Pmin /kW	Pmax /kW	Uphill/downhill /kW/h	Maintenance cost /RMB/kW
CCHP	P_e	500	1000	200	0.1
	P_h	750	1500	—	—
	P_c	0	500	—	0.02
GB		100	500	100	0.012
ER		0	100	—	0.015
HP		0	200	—	0.006
PV		0	400	—	0.0235

TABLE 3. The parameters of energy storage equipment in each energy station.

Storage	ES	HS	CS
Cap/kWh	800	200	200
$\gamma_{(g)}^{dis}$	0.2	0.2	0.2
$\eta_{(g)}^{cha}$	0.90	0.98	0.95
SOC^{min}	0.2	0.2	0.2
SOC^{max}	0.9	0.9	0.9

TABLE 4. The energy network parameters of each energy station.

Node number		Line number	Length (km)
Beginning	End		
1	2	1	1
1	3	2	1.5
2	4	3	2
3	5	4	1

The purchase prices for three periods are 0.17 RMB/kWh, 0.49RMB/kWh and 0.83RMB/kWh, and the selling prices for three periods are 0.13RMB/kWh, 0.38RMB/kWh and 0.65RMB/kWh, respectively. The surplus energy of the integrated energy system can be sold to the power grid, and the TOU price is also adopted. The price of natural gas is 2.5 yuan/m3. The power factor of the power transmission between energy stations is 0.85. It is assumed that the reactive power compensation device of each energy station can keep this power factor unchanged.

The impedance of power line per unit length is 0.0080 + j0.0056 (p.u.). The transmission lines of the four sections are the same. The maximum transmission power of the lines is 1MVA, and the maximum node voltage deviation is ±5%. The pipeline coefficient of natural gas is 80. The minimum value of gas pressure at pipeline nodes is 100 Mpa, and the maximum value is 10 Mpa. The friction resistance coefficient of hot water pipeline is 2°C/km.

TABLE 5. The operation costs of five energy stations before considering the power load demand response Unit: RMB.

Energy station		ES1	ES2	ES3	ES4	ES5
Electricity prices	Buy	2351	2055	2208	309	129
	Sale	1253	1186	1555	1315	2380
	Total	1098	869	653	-1006	-2251
Fuel cost		12754	8692	10257	12794	11732
Start and stop cost		12	10	5	8	0
Maintenance cost		1857	1275	1457	1845	1736
Total cost		**15722**	**10846**	**12372**	**13642**	**11218**

TABLE 6. The operation costs of five energy stations after considering the power load demand response Unit: RMB.

Energy station		ES1	ES2	ES3	ES4	ES5
Electricity prices	Buy	2316	2127	1908	384	145
	Sale	1581	1423	1764	1565	2619
	Total	735	704	144	-1181	-2474
Fuel cost		12860	8651	10397	12788	11801
Start and stop cost		12	10	5	8	0
Maintenance cost		1895	1259	1500	1844	1746
Demand response revenue		204	163	178	124	95
Total cost		**15298**	**10460**	**11868**	**13335**	**10979**

B. THE INFLUENCE OF ELECTRIC LOAD DEMAND RESPONSE ON INDEPENDENT OPERATION COST OF ENERGY STATION

This section analyzes the impacts of demand response on integrated energy system operation. Each energy station is assumed to be optimized independently. Table 5 shows the optimization results without demand response, and Table 6 shows the corresponding results in consideration of demand response.

The operating costs of five energy stations before participating in demand response are 10846 RMB to 15722 RMB, and the costs after participating in demand response are 10460 RMB to 15298 RMB. It is observed that the scenarios with demand response have smaller optimization objectives, indicating an operating point with the less operational cost. For example, the operational cost of the third energy station with demand response is reduced by 4.07% compared to the scenario without demand response. The operational cost of the fifth energy station with demand response is reduced by 2.13%. The results show that demand response of different kinds of loads contributes to a more optimal operating point with the less operational cost.

C. COMPARISON OF THE OPERATION COSTS OF INTEGRATED ENERGY SYSTEM BEFORE AND AFTER CONSIDERING THE DEMAND RESPONSE AND THE PHOTOVOLTAIC OUTPUT UNCERTAINTY

This section analyzes the impacts of photovoltaic uncertainty and demand response on integrated energy system operation. Five scenarios are compared with each other, and the five scenarios are listed as follows.

Scenario 1: Five energy stations are optimized independently without consideration of photovoltaic uncertainty and demand response;

TABLE 7. The independent and cooperative operation costs of energy station Unit: RMB.

Scenario		1	2	3	4	5
Electricity prices	Buy	6880	6469	5866	6383	5357
	Sale	8952	0	0	0	0
	Total	-2072	6469	5866	6383	5357
Fuel cost		56497	38350	38860	38638	39519
Start and stop cost		35	15	9	15	15
Maintenance cost		8244	6268	6336	6307	6427
Demand response revenue		764	0	384	0	385
Total cost		**61940**	**51101**	**50686**	**51343**	**50933**

Scenario 2: Five energy stations are optimized coordinately without consideration of photovoltaic uncertainty and demand response;

Scenario 3: Five energy stations are optimized coordinately in consideration of demand response but with consideration of photovoltaic uncertainty;

Scenario 4: Five energy stations are optimized coordinately in consideration of photovoltaic uncertainty but without consideration of demand response;

Scenario 5: Five energy stations are optimized coordinately in consideration of photovoltaic uncertainty and demand response.

The operational costs of the five scenarios are listed in Table 7. It is observed that the scenario 1 has the highest operational cost, i.e., 61940RMB, which is 21.2% higher than the cost of the scenario 2. This shows that coordinated operation of different energy stations can have a better operating point with the less operational cost. For all scenarios, the scenario 3 has the minimum operational cost with coordinated operation and demand response, and the corresponding cost is 415RMB less than the scenario 2, indicating demand response has a positive impact on the system operation. Compared to the scenario 2, the scenario 4 has a larger operational cost due to photovoltaic uncertainty. Compared to the scenario 3, the scenario 5 has a larger operational cost also due to photovoltaic uncertainty. However, the scenario 5 has a less operational cost also due to demand response.

In case 5, considering the demand response of electric load and the uncertainty of photovoltaic output, the transmission power of the power line between multi-energy stations in the integrated energy system in each period is shown in Fig. 8. The No.1 energy station located in the regional center is connected to the external power grid. As a balance node, its voltage value is assumed to be 1 and remains unchanged. The power delivered by the integrated energy system to the power grid is 0 and the system stops purchasing power from the grid during the peak period of the electricity price. The peak electricity price period corresponds to the peak period of the grid load, which shows that the integrated energy system can play a good role in peak shaving of the grid. This is mainly because there are distributed power generation equipment and multi-energy storage equipment in the integrated energy system. No.5 energy station has transferred a lot of power to the system.

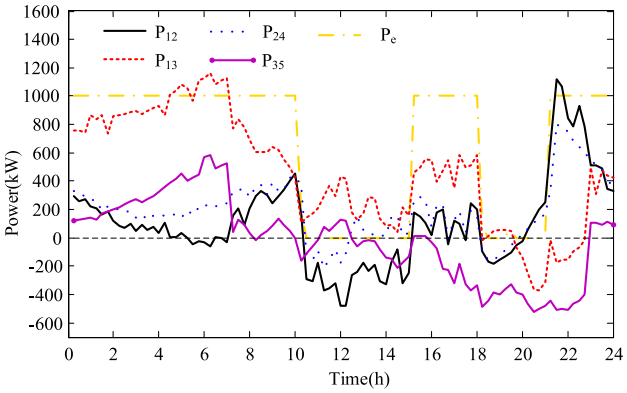

FIGURE 8. Transmission power of power lines between multi-energy stations in integrated energy system.

VI. CONCLUSION

In this paper, a coordinated optimal scheduling of the integrated energy systems including multi-energy stations is investigated. The main equipment model of integrated energy system is established. The characteristics of energy transmission network between multi-energy stations are analyzed, and the linearization model of multi-energy network is constructed. Taking into account the uncertainty caused by the accessing of photovoltaic power to the integrated energy system, the sampling and scenario reduction methods are used to generate typical scenarios to determine the uncertainty value range of photovoltaic output and set the uncertainty range of the robust optimization. Considering the participation of multi-energy users electric load in the demand response of electric energy, a robust optimization model is established, in order to improves the energy supply economy of the terminal integrated energy system and the operation safety. Through case simulation, it is proved that the proposed multi-energy station collaborative optimization scheduling strategy of the integrated energy system has higher economy of energy supply than single energy station operation. The next step is to combine the robust optimization with the intraday rolling optimization to improve the response speed and operation economy of the integrated energy system, and to connect the dispatch of the real-time energy utilization.

REFERENCES

[1] M. Geidl, G. Koeppel, P. Favre-Perrod, B. Klockl, G. Andersson, and K. Frohlich, "Energy hubs for the future," *IEEE Power Energy Mag.*, vol. 5, no. 1, pp. 24–30, Jan. 2007.

[2] J. Wang, H. Zhong, C.-W. Tan, X. Chen, R. Rajagopal, Q. Xia, and C. Kang, "Economic benefits of integrating solar-powered heat pumps into a CHP system," *IEEE Trans. Sustain. Energy*, vol. 9, no. 4, pp. 1702–1712, Oct. 2018.

[3] C. Wang, C. Lv, P. Li, G. Song, S. Li, X. Xu, and J. Wu, "Modeling and optimal operation of community integrated energy systems: A case study from China," *Appl. Energy*, vol. 230, pp. 1242–1254, Nov. 2018.

[4] X. Chen, C. Kang, M. O'Malley, Q. Xia, J. Bai, C. Liu, R. Sun, W. Wang, and H. Li, "Increasing the flexibility of combined heat and power for wind power integration in China: Modeling and implications," *IEEE Trans. Power Syst.*, vol. 30, no. 4, pp. 1848–1857, Jul. 2015.

[5] G. Li, R. Zhang, T. Jiang, H. Chen, L. Bai, H. Cui, and X. Li, "Optimal dispatch strategy for integrated energy systems with CCHP and wind power," *Appl. Energy*, vol. 192, pp. 408–419, Apr. 2017.

[6] A. Hellmers, M. Zugno, A. Skajaa, and J. M. Morales, "Operational strategies for a portfolio of wind farms and CHP plants in a two-price balancing market," *IEEE Trans. Power Syst.*, vol. 31, no. 3, pp. 2182–2191, May 2016.

[7] J.-J. Wang, Y.-Y. Jing, and C.-F. Zhang, "Optimization of capacity and operation for CCHP system by genetic algorithm," *Appl. Energy*, vol. 87, no. 4, pp. 1325–1335, Apr. 2010.

[8] X. Zheng, G. Wu, Y. Qiu, X. Zhan, N. Shah, N. Li, and Y. Zhao, "A MINLP multi-objective optimization model for operational planning of a case study CCHP system in urban China," *Appl. Energy*, vol. 210, pp. 1126–1140, Jan. 2018.

[9] G. K. H. Larsen, N. D. van Foreest, and J. M. A. Scherpen, "Distributed MPC applied to a network of households with micro-CHP and heat storage," *IEEE Trans. Smart Grid*, vol. 5, no. 4, pp. 2106–2114, Jul. 2014.

[10] H. Ren and W. Gao, "A MILP model for integrated plan and evaluation of distributed energy systems," *Appl. Energy*, vol. 87, no. 3, pp. 1001–1014, Mar. 2010.

[11] K. Hossein, M. J. Sanjari, S. H. Hosseinian, and G. B. Gharehpetian, "An optimal dispatch algorithm for managing residential distributed energy resources," *IEEE Trans. Smart Grid*, vol. 5, no. 5, pp. 2367–2360, Sep. 2014.

[12] D. J. Olsen, N. Zhang, C. Kang, M. A. Ortega-Vazquez, and D. S. Kirschen, "Planning low-carbon campus energy hubs," *IEEE Trans. Power Syst.*, vol. 34, no. 3, pp. 1895–1907, May 2019.

[13] T. C. Fubara, F. Cecelja, and A. Yang, "Modelling and selection of micro-CHP systems for domestic energy supply: The dimension of network-wide primary energy consumption," *Appl. Energy*, vol. 114, pp. 327–334, Feb. 2014.

[14] D. Xie, A. Chen, C. Gu, and J. Tai, "Time-domain modeling of grid-connected CHP for its interaction with the power grid," *IEEE Trans. Power Syst.*, vol. 33, no. 6, pp. 6430–6440, Nov. 2018.

[15] K. Zhou, J. Pan, and L. Cai, "Indirect load shaping for CHP systems through real-time price signals," *IEEE Trans. Smart Grid*, vol. 7, no. 1, pp. 282–290, Jan. 2016.

[16] S. Heinen and M. J. O'Malley, "Complementarities of supply and demand sides in integrated energy systems," *IEEE Trans. Smart Grid*, vol. 10, no. 1, pp. 1156–1165, Jan. 2019.

[17] Y. Dai, L. Chen, Y. Min, Q. Chen, K. Hu, J. Hao, Y. Zhang, and F. Xu, "Dispatch model of combined heat and power plant considering heat transfer process," *IEEE Trans. Sustain. Energy*, vol. 8, no. 3, pp. 1225–1236, Jul. 2017.

[18] W. Gu, J. Wang, S. Lu, Z. Luo, and C. Wu, "Optimal operation for integrated energy system considering thermal inertia of district heating network and buildings," *Appl. Energy*, vol. 199, pp. 234–246, Aug. 2017.

[19] J. Yang, N. Zhang, Y. Cheng, C. Kang, and Q. Xia, "Modeling the operation mechanism of combined P2G and gas-fired plant with CO2 recycling," *IEEE Trans. Smart Grid*, vol. 10, no. 1, pp. 1111–1121, Jan. 2019.

[20] C. Wang, Z. Wang, Y. Hou, and K. Ma, "Dynamic game-based maintenance scheduling of integrated electric and natural gas grids with a bilevel approach," *IEEE Trans. Power Syst.*, vol. 33, no. 5, pp. 4958–4971, Sep. 2018.

[21] E. A. Martinez Cesena and P. Mancarella, "Energy systems integration in smart districts: Robust optimisation of multi-energy flows in integrated electricity, heat and gas networks," *IEEE Trans. Smart Grid*, vol. 10, no. 1, pp. 1122–1131, Jan. 2019.

[22] A. Baringo, L. Baringo, and J. M. Arroyo, "Day-ahead self-scheduling of a virtual power plant in energy and reserve electricity markets under uncertainty," *IEEE Trans. Power Syst.*, vol. 34, no. 3, pp. 1881–1894, May 2019.

[23] R. Mohammadi, H. R. Mashhadi, and M. Shahidehpour, "Market-based customer reliability provision in distribution systems based on game theory: A bi-level optimization approach," *IEEE Trans. Smart Grid*, vol. 10, no. 4, pp. 3840–3848, Jul. 2019.

[24] Y. Jiang, J. Xu, Y. Sun, C. Wei, J. Wang, D. Ke, X. Li, J. Yang, X. Peng, and B. Tang, "Day-ahead stochastic economic dispatch of wind integrated power system considering demand response of residential hybrid energy system," *Appl. Energy*, vol. 190, pp. 1126–1137, Mar. 2017.

[25] C. Wu, W. Gu, R. Bo, P. Jiang, Z. Wu, S. Lu, and S. Yao, "A two-stage game model for combined heat and power trading market," *IEEE Trans. Power Syst.*, vol. 34, no. 1, pp. 506–517, Jan. 2019.

[26] F. Valencia, J. Collado, D. Saez, and L. G. Marin, "Robust energy management system for a microgrid based on a fuzzy prediction interval model," *IEEE Trans. Smart Grid*, vol. 7, no. 3, pp. 1486–1494, May 2016.

[27] W. van Ackooij, E. C. Finardi, and G. M. Ramalho, "An exact solution method for the hydrothermal unit commitment under wind power uncertainty with joint probability constraints," *IEEE Trans. Power Syst.*, vol. 33, no. 6, pp. 6487–6500, Nov. 2018.

[28] L. Exizidis, J. Kazempour, A. Papakonstantinou, P. Pinson, Z. De Greve, and F. Vallee, "Incentive-compatibility in a two-stage stochastic electricity market with high wind power penetration," *IEEE Trans. Power Syst.*, vol. 34, no. 4, pp. 2846–2858, Jul. 2019.

[29] J. Aghaei, V. G. Agelidis, M. Charwand, F. Raeisi, A. Ahmadi, A. E. Nezhad, and A. Heidari, "Optimal robust unit commitment of CHP plants in electricity markets using information gap decision theory," *IEEE Trans. Smart Grid*, vol. 8, no. 5, pp. 2296–2304, Sep. 2017.

[30] M. Majidi and K. Zare, "Integration of smart energy hubs in distribution networks under uncertainties and demand response concept," *IEEE Trans. Power Syst.*, vol. 34, no. 1, pp. 566–574, Jan. 2019.

[31] B. V. Solanki, A. Raghurajan, K. Bhattacharya, and C. A. Canizares, "Including smart loads for optimal demand response in integrated energy management systems for isolated microgrids," *IEEE Trans. Smart Grid*, vol. 8, no. 4, pp. 1739–1748, Jul. 2017.

[32] C. Shao, Y. Ding, J. Wang, and Y. Song, "Modeling and integration of flexible demand in heat and electricity integrated energy system," *IEEE Trans. Sustain. Energy*, vol. 9, no. 1, pp. 361–370, Jan. 2018.

[33] A. Sheikhi, M. Rayati, S. Bahrami, and A. M. Ranjbar, "Integrated demand side management game in smart energy hubs," *IEEE Trans. Smart Grid*, vol. 6, no. 2, pp. 675–683, Mar. 2015.

[34] H. Gao, L. Wang, J. Liu, and Z. Wei, "Integrated day-ahead scheduling considering active management in future smart distribution system," *IEEE Trans. Power Syst.*, vol. 33, no. 6, pp. 6049–6061, Nov. 2018.

[35] M. E. Baran and F. F. Wu, "Network reconfiguration in distribution systems for loss reduction and load balancing," *IEEE Trans. Power Del.*, vol. 4, no. 2, pp. 1401–1407, Apr. 1989.

[36] J. A. Taylor and F. S. Hover, "Convex models of distribution system reconfiguration," *IEEE Trans. Power Syst.*, vol. 27, no. 3, pp. 1407–1413, Aug. 2012.

[37] S. Lei, Y. Hou, F. Qiu, and J. Yan, "Identification of critical switches for integrating renewable distributed generation by dynamic network reconfiguration," *IEEE Trans. Sustain. Energy*, vol. 9, no. 1, pp. 420–432, Jan. 2018.

[38] B. Wang, P. Dehghanian, and D. Zhao, "Chance-constrained energy management system for power grids with high proliferation of renewables and electric vehicles," *IEEE Trans. Smart Grid*, vol. 11, no. 3, pp. 2324–2336, May 2020.

[39] M. Robert and D. Yury, "Distribution electricity pricing under uncertainty," *IEEE Trans. Power Syst.*, vol. 35, no. 3, pp. 2325–2338, May 2020.

[40] K. N. Hasan, R. Preece, and J. V. Milanović, "Existing approaches and trends in uncertainty modelling and probabilistic stability analysis of power systems with renewable generation," *Renew. Sustain. Energy Rev.*, vol. 101, pp. 168–180, Mar. 2019.

[41] G. Mavromatidis, K. Orehounig, and J. Carmeliet, "A review of uncertainty characterisation approaches for the optimal design of distributed energy systems," *Renew. Sustain. Energy Rev.*, vol. 88, pp. 258–277, May 2018.

[42] H. Zhou, Z. Li, J. H. Zheng, Q. H. Wu, and H. Zhang, "Robust scheduling of integrated electricity and heating system hedging heating network uncertainties," *IEEE Trans. Smart Grid*, vol. 11, no. 2, pp. 1543–1555, Mar. 2020.

[43] Y. Zhou, M. Shahidehpour, Z. Wei, Z. Li, G. Sun, and S. Chen, "Distributionally robust unit commitment in coordinated electricity and district heating networks," *IEEE Trans. Power Syst.*, vol. 35, no. 3, pp. 2155–2166, May 2020.

[44] A. R. Sayed, C. Wang, J. Zhao, and T. Bi, "Distribution-level robust energy management of power systems considering bidirectional interactions with gas systems," *IEEE Trans. Smart Grid*, vol. 11, no. 3, pp. 2092–2105, May 2020.

JINGJING ZHAI was born in Tangshan, Hebei, China, in 1982. She received the B.S. degree in electrical engineering from the Nanjing University of Science and Technology, in 2004, and the M.S. degree in electrical engineering from Southeast University, in 2007. She is currently pursuing the Ph.D. degree in control engineering with the Nanjing University of Science and Technology.

From 2007 to 2012, she worked with the Nanjing NARI Group Company. Since 2013, she has been a Laboratory Technician with the Nanjing Institute of Technology. Her research interests include integrated energy system optimal operation and smart power utilization.

XIAOBEI WU was born in Chengdu, Sichuan, China, in 1958. She received the B.S. and M.S. degrees in automation control from the Nanjing University of Science and Technology, in 1982 and 1984, respectively.

Since 1984, she has successively been an Assistant Professor and a Professor with the College of Automation, Nanjing University of Science and Technology. She is the author of more than 80 articles. Her research interests include wireless sensor networks and intelligent control technology.

Prof. WU is the Vice-Chairman of the Automation Specialty Teaching Guiding Committee of the Ministry of Education of China and the Standing Council Member of Artificial Intelligence (AI) Society of China.

SHAOJIE ZHU was born in Xiangyang, Hubei, China, in 1994. He received the B.S. degree in electrical engineering from Guizhou University, in 2017. He is currently pursuing the M.S. degree in electrical engineering with Hohai University.

BO YANG was born in Jiangyin, Jiangsu, China, in 1977. He received the B.S. and M.S. degrees in electrical engineering from Southeast University, in 2000 and 2003, respectively, where he is currently pursuing the Ph.D. degree in electrical engineering.

From 2007 to 2012, he worked with the Nanjing NARI Group Company. In 2012, he was transferred to the New Energy Center, China Electric Power Research Institute, as the Director of the Energy Storage Application Technology Laboratory. He is also currently serving as an Industry Professor with Hohai University and an off-campus Master Tutor with Southeast University. He is the author of three books, more than 20 articles, and more than 12 inventions. His research interests include power electronics technology, energy storage, converter and integration, micro grid integration technology research, and product development.

HAOMING LIU (Senior Member, IEEE) was born in Yancheng, Jiangsu, China, in 1977. He received the B.S., M.S., and Ph.D. degrees in electrical engineering from the Nanjing University of Science and Technology, Nanjing, China, in 1998, 2001, and 2003, respectively.

From 2004 to 2005, he was a Postdoctoral Fellow with Southeast University, Nanjing. Since 2006, he has successively been an Associate Professor and a Professor with the College of Energy and Electrical Engineering, Hohai University, Nanjing. He is the author of one book, more than 200 articles, and more than ten inventions. His research interests include new energy generation, distribution system analysis and control, and electricity market.